

1 **Tailoring the Local Environment of Platinum in Single-Atom Pt₁/CeO₂ Catalysts for**
2 **Robust Low-Temperature CO Oxidation**

3
4
5 *Dong Jiang,¹ Yonggang Yao,² Tangyuan Li,² Gang Wan,³ Xavier Isidro Pereira-Hernández,¹*
6 *Yubing Lu,⁴ Jinshu Tian,⁴ Konstantin Khivantsev,⁴ Mark H. Engelhard,⁴ Chengjun Sun,⁵*
7 *Carlos E. García-Vargas,¹ Adam S. Hoffman,³ Simon R. Bare,³ Abhaya K. Datye,^{6*} Liangbing*
8 *Hu,^{2*} and Yong Wang^{1,4*}*

9
10
11 Dr. D. Jiang, Dr. X. I. Pereira-Hernández, C. E. García-Vargas, Prof. Y. Wang
12 The Gene and Linda Voiland School of Chemical Engineering and Bioengineering,
13 Washington State University, Pullman, WA 99164, USA.
14 E-mail: yong.wang@pnnl.gov

15
16 Dr. Y. G. Yao, T. Y. Li, Prof. L. B. Hu
17 Department of Materials Science and Engineering, University of Maryland, College Park,
18 MD, 20742, USA.
19 E-mail: binghu@umd.edu

20
21 Dr. Y. G. Yao
22 Current address:
23 State Key Laboratory of Materials Processing and Die & Mould Technology
24 School of Materials Science and Engineering
25 Huazhong University of Science and Technology
26 Wuhan, 430074, China

27
28 Dr. G. Wan, Dr. A. D. Hoffman, Dr. S. R. Bare
29 Stanford Synchrotron Radiation Lightsource, SLAC National Accelerator Laboratory, Menlo
30 Park, CA 94025, USA.

31
32 Dr. Y. B. Lu, Dr. J. S. Tian, Dr. K. Khivantsev, Dr. M. H. Engelhard, Prof. Y. Wang
33 Institute for Integrated Catalysis, Pacific Northwest National Laboratory, Richland, WA
34 99354, USA.

35
36 Dr. C. J. Sun
37 X-ray Science Division, Advanced Photon Source, Argonne National Laboratory, Lemont, IL
38 60439, USA.

39
40 Prof. A. K. Datye
41 Department of Chemical and Biological Engineering and Center for Micro-Engineered
42 Materials, University of New Mexico, Albuquerque, NM 87131, USA.
43 E-mail: datye@unm.edu

44
45
46 **Keywords:** single-atom catalysis, thermal-shock synthesis, CO oxidation, platinum, metal-
47 support interactions.

1 **Abstract**

2 Single-atom Pt₁/CeO₂ catalyst by atom trapping (AT, 800 °C in air) shows excellent thermal
3 stability, however, it is inactive for CO oxidation at low temperatures due to over-stabilization
4 of Pt²⁺ in a highly symmetric square-planar Pt₁O₄ coordination. Reductive activation forming
5 Pt nanoparticles (NPs) results in enhanced activity, however, NPs are easily oxidized leading
6 to drastic activity loss. Here we show that tailoring the local environment of isolated Pt²⁺ via
7 thermal-shock (TS) synthesis leads to a highly active and thermally stable Pt₁/CeO₂ catalyst.
8 Ultrafast shockwaves (> 1200 °C) in an inert atmosphere induce surface reconstruction of
9 CeO₂, generating Pt single atoms in an asymmetric Pt₁O₄ configuration. Originating from this
10 unique coordination, Pt₁^{δ+} in a partially reduced state dynamically evolved during CO
11 oxidation, resulting in an exceptional low-temperature performance. The CO oxidation
12 reactivity on the Pt₁/CeO₂_TS catalyst is retained under oxidizing conditions.

13
14
15
16
17
18
19
20
21
22
23
24
25
26
27
28
29
30
31
32
33
34
35
36
37
38
39

1 **1. Introduction**

2 Supported precious metals with atomic dispersion have proved promising for achieving
3 maximum atom efficiency as well as improved activity and selectivity in catalyzing a growing
4 number of thermo-, electro-, and photo- driven chemical reactions.[1] A major challenge for
5 single atom catalysts (SACs) in future industrial applications is attaining high reactivity while
6 simultaneously demonstrating high thermal stability.

7 CO oxidation is industrially important in vehicle emission control, requiring catalysts with
8 high reactivity (high concentrations of active sites) as well as thermal stability.[2] Single-atom
9 Pt₁/CeO₂ has been widely studied for emission control applications.^[1a, 3] To achieve high
10 thermal stability at high metal loadings (≥ 1 wt %), Pt atoms need to form strong covalent
11 bonds with the support.^[1a, 3a, 4] For instance, we developed an atom trapping (AT) method, i.e.,
12 heat treatment at 800 °C in air,^[1a] allowing volatile PtO₂ to be trapped at the most
13 thermodynamically stable binding sites, e.g., monoatomic CeO₂ (111) step edges.^[3a, 3b] Using
14 this approach, we recently reported the synthesis of thermally stable Pt₁/CeO₂ catalysts at Pt
15 loadings of up to 3 wt %.^[3a] In these catalysts, Pt adopts a highly symmetric square-planar
16 Pt₁O₄ coordination, which can be expected from the crystal field theory for a Pt²⁺ d⁸ electronic
17 configuration.^[3g, 5] Such an over-stabilization results in a greatly compromised ability of
18 isolated Pt²⁺ for activating gas-phase molecules (e.g., CO, H₂),^[5b, 6] making them nearly
19 inactive for CO oxidation below 200 °C.^[1a, 7] A common feature of these strongly bonded Pt
20 single atoms is that they require some form of activation (e.g., reduction in CO/H₂, or
21 treatment in steam) to achieve enhanced low temperature CO oxidation performance.^[3c-e, 7-8]
22 The highest activity is obtained when ionic Pt single atoms are transformed into metallic
23 clusters/NPs.^[3e, 7, 8b] However, when exposed to oxidizing conditions at elevated temperatures,
24 Pt clusters/NPs break up into single atoms that revert to a low activity state.^[3e, 7] This is much
25 less desirable for the application of these SACs in emission control systems, especially during
26 the cold-start of engines. Hence, there is an urgent need to develop single-atom Pt₁/CeO₂

1 catalysts that demonstrate CO oxidation activity at low temperatures, and at the same time are
2 resistant to the activity loss under oxidizing conditions.

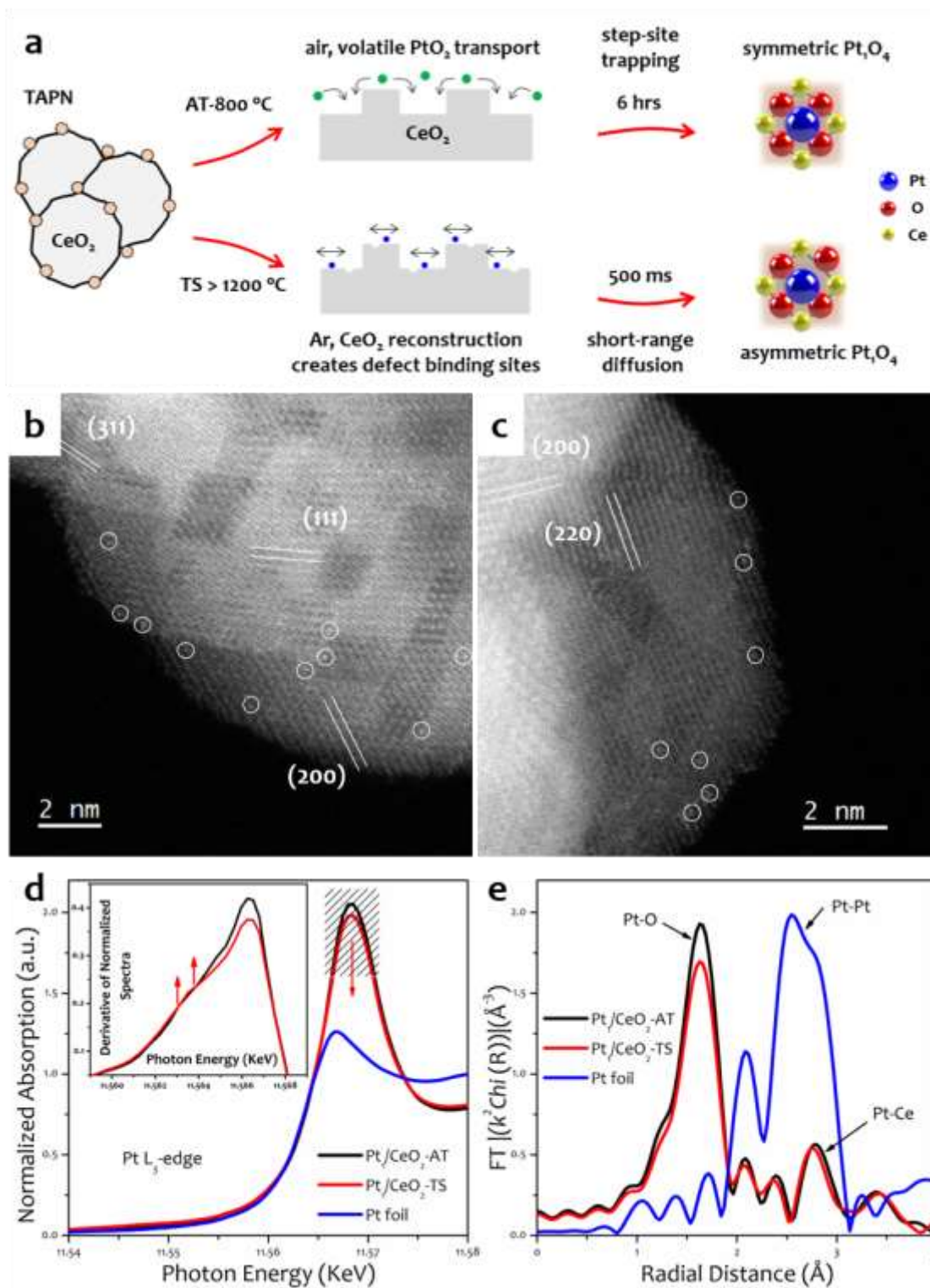
3 The distinct behavior of single atoms from that of NPs stems from the unique local
4 coordination environment of isolated metal atoms, as well as their interactions with the
5 support.^[9] Therefore, insights into the coordination and electronic states of supported single
6 atoms as well as their dynamic changes under reaction conditions are crucial for unraveling
7 the precise structure-function relationships of SACs.^[3h, 10] For instance, DeRita et al.
8 demonstrated that under varied redox conditions isolated Pt on TiO₂ can adopt a range of local
9 coordination and oxidation states, showing a strong influence on CO oxidation reactivity.^[10c]
10 Similarly, Tang et al. confirmed that Rh single atoms adapt their local coordination under
11 various redox conditions, including calcination in O₂, reduction in H₂, and reverse water gas
12 shift (RWGS) reaction.^[10d] To achieve high thermal stability, these authors used very low
13 loadings of metals (0.025-0.05 wt %) so that agglomeration of isolated metal atoms could be
14 avoided.^[3g, 9a, 10c]

15 Here we demonstrate single-atom Pt₁/CeO₂ catalyst at an industrially relevant loading (1
16 wt %) that is oxidation resistant and reactive for low-temperature CO oxidation can be
17 achieved by tailoring the local environment of isolated Pt sites. In particular, single-atom
18 Pt₁/CeO₂ was synthesized by a thermal-shock (TS) method to tailor the Pt-CeO₂ interaction,
19 i.e., the local coordination and electronic states of isolated Pt on CeO₂. The TS synthesis has
20 been developed for stabilizing high-entropy-alloy NPs as well as metal single atoms on
21 different supports (e.g., carbon, C₃N₄, and TiO₂).^[11] Here, controlled high-temperature (>
22 1200 °C) shockwaves are produced via a periodic on-off heating that consists of a short on-
23 state (~ 500 ms) and a 6-times longer off-state (Figure S1). The high-temperature flash
24 heating drives Pt dispersion by restructuring the CeO₂ surface and making it suitable for
25 forming strong Pt-O-Ce bonding, while the rapid cooling (~ 10⁴ K/s) off-state prevents the
26 sintering of Pt and CeO₂. Furthermore, by performing TS in an inert atmosphere, vapor-phase

1 transport of PtO₂ is largely limited, allowing Pt atoms to be stabilized at sites different from
2 the most thermodynamically stable square-planar pockets at CeO₂ step edges. As a result,
3 stable Pt²⁺ single atoms in an asymmetric Pt₁O₄ configuration are formed (Figure 1a).
4 Originating from such asymmetric local coordination, partially reduced Pt₁^{δ+} species in Pt₁O₄-
5_x configurations are induced during CO oxidation, leading to a significantly superior low-
6 temperature activity compared to Pt₁/CeO₂ synthesized via atom trapping (AT).

7 **2. Results and Discussion**

8 As illustrated in Figure 1a, tetraammineplatinum nitrate (TAPN) as the Pt precursor was
9 introduced onto CeO₂ by incipient wetness impregnation (IWI), followed by AT and TS
10 treatments to obtain the Pt₁/CeO₂_AT and Pt₁/CeO₂_TS catalysts with 1 wt % Pt loading,
11 respectively. The absence of X-ray diffraction for Pt/PtO₂ (Figure S2) indicates the high
12 dispersion of Pt on CeO₂. Atomic dispersion of Pt was confirmed by aberration-corrected
13 scanning transmission electron microscopy (AC-STEM) in the high-angle annular dark-field
14 (HAADF) imaging mode, where only isolated Pt atoms can be observed in both catalysts
15 (Figures 1b and 1c). Since the two methods employed the same precursor (i.e., TAPN
16 deposited on polyhedral CeO₂ obtained by calcination of cerium nitrate), both Pt₁/CeO₂
17 catalysts present multiple nanofacets (e.g., {111}, {110}, and {100}) without noticeable
18 difference (Figures S3 and S4). The BET surface areas were measured to be 40.0 m²/g for
19 Pt₁/CeO₂_AT and 67.1 m²/g for Pt₁/CeO₂_TS (Table S1). Compared to atom-trapping which
20 requires prolonged heating at 800 °C, the ultrafast pulse heating and cooling helps preserve
21 the surface area of the CeO₂ support (Figure 1a).^[11a, 11b] In addition, this thermal-shock
22 method shows much superior cost-effectiveness to conventional furnace calcination in terms
23 of the energy and time spent for catalyst preparation (Table S2).



1
2
3 **Figure 1.** (a) Schematic of the AT and TS synthesis of single-atom 1wt % Pt₁/CeO₂ catalysts
4 showing the symmetric (near-perfect) and asymmetric (distorted square-planar) Pt₁O₄
5 coordination in Pt₁/CeO₂_AT and Pt₁/CeO₂_TS, respectively. AC-STEM images of as-
6 synthesized Pt₁/CeO₂_AT (b) and Pt₁/CeO₂_TS (c) showing the exclusive presence of isolated
7 Pt atoms. Pt L₃-edge XANES (d) and Fourier transform of *k*²-weighted EXAFS (e) of as-
8 synthesized Pt₁/CeO₂ catalysts and the Pt foil reference. Inset of (d) is the 1st derivative of the
9 normalized XANES in (d).
10

1 The single-atom nature of supported Pt was further investigated by X-ray absorption
2 spectroscopy (XAS) at Pt L₃-edge which provides information on the oxidation state and the
3 local coordination environment of Pt.^[3a, 4a, 12] Figure 1d shows the X-ray absorption near edge
4 structure (XANES) spectra of Pt foil and as-synthesized Pt₁/CeO₂ catalysts in an air-exposed
5 state. The white line intensity of Pt₁/CeO₂_TS is much higher than that of Pt foil but is close
6 to that of Pt₁/CeO₂_AT which has been proven to exclusively contain isolated and ionic Pt
7 species in a mixed +2/+4 charge state (Pt²⁺ is dominant).^[3a, 7] Given the absence of Pt-Pt
8 scattering as clearly indicated in the extended X-ray absorption fine structure (EXAFS), the
9 as-synthesized Pt₁/CeO₂_TS is also dominated by isolated Pt²⁺ cations (Figure 1e). This is
10 also confirmed by X-ray photoelectron spectroscopy (XPS) in the Pt 4f region (Figure S5a). It
11 should be noted that compared to Pt₁/CeO₂_AT, Pt₁/CeO₂_TS shows a slightly lower white
12 line intensity (Figure 1d), suggesting a slightly more reduced valence state or coordination
13 symmetry of ionic Pt²⁺.^[13] More importantly, there appears a rising-edge feature above the
14 XANES absorption edge of Pt₁/CeO₂_TS, evidenced by a bump in the first-order derivative
15 curve (inset of Figure 1d). Appearance of such rising edge is believed to be associated with
16 the decreased local coordination symmetry around Pt sites.^[14] This confirms our initial
17 speculation that TS produces isolated Pt²⁺ with an asymmetric Pt₁O₄ configuration (Figure
18 1a).

19 **Table 1.** Best fitting results of EXAFS over as-synthesized Pt₁/CeO₂_AT and Pt₁/CeO₂_TS).
20

	Scattering pair	CN	R (Å)	σ ² (Å ²)	R factor	Comment
Pt ₁ /CeO ₂ _AT	Pt-O	4 (fixed)	1.995	0.00119	0.0074	symmetric (near-perfect square-planar) Pt ₁ O ₄
Pt ₁ /CeO ₂ _TS	Pt-O _S ^a	3 (fixed)	1.979	0.00112	0.00592	asymmetric (distorted square-planar) Pt ₁ O ₄
	Pt-O _L ^b	1 (fixed)	2.051	0.00070		

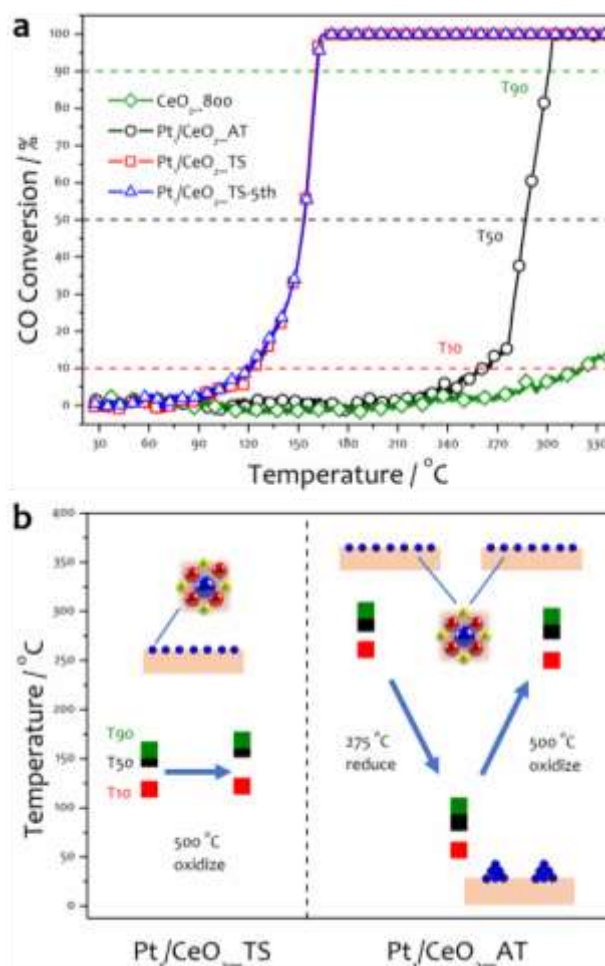
21
22 ^a) O_S is lattice oxygen of CeO₂ bonded to Pt with a shorter Pt-O bond length. ^b) O_L is oxygen
23 atom at a longer distance, possibly lattice oxygen or foreign oxygen atoms from surface
24 hydroxyls (-OH) or chemisorbed O*.

25

1 The local coordination environments of isolated Pt^{2+} in the two Pt_1/CeO_2 catalysts were
2 analyzed by carefully fitting the EXAFS spectra (Figure S6). As summarized (Table 1),
3 $\text{Pt}_1/\text{CeO}_2_{\text{AT}}$ can be readily fitted with a near-perfect square-planar Pt_1O_4 configuration with
4 four equivalent Pt-O bonds, which is preferred by Pt^{2+} as a d^8 ion.^[3g, 5a] For $\text{Pt}_1/\text{CeO}_2_{\text{TS}}$,
5 employing the same high-symmetry model led to a Pt-O coordination number (CN) of ~ 3.5
6 (Table S3), indicating a defect Pt_1O_3 motif. This is not reasonable for the air-exposed state
7 since it has been proposed that excess Pt-O bonds will form from ambient O_2 once there is a
8 vacancy (O_V), resulting in a $\text{CN} > 4$.^[3a, 10e] Instead, improved fitting results were obtained
9 from an asymmetric square-planar Pt_1O_4 geometry with three shorter Pt-Os of 1.979 Å and
10 one longer Pt-O_L of 2.051 Å, which likely involves surface hydroxyls (-OH) or chemisorbed
11 O^* as suggested by the O 1s XPS results (Figure S5b). A similar structure has been proposed
12 for isolated Pt^{2+} on top of anatase TiO_2 due to its tetragonal crystalline structure,^[3g, 9a] which can
13 be expected here considering the binding sites created by the TS-induced surface
14 reconstruction of CeO_2 . Therefore, based on above combined XANES (Figure 1d) and
15 EXAFS (Figure 1e) analysis, compared to AT that produced a near-perfect square-planar
16 Pt_1O_4 coordination, an asymmetric Pt_1O_4 geometry was formed by the TS treatment. This
17 further confirms our initial hypothesis (Figure 1a) and suggests that isolated Pt formed by TS
18 is located in a different surface site of CeO_2 compared to that prepared by AT.

19 The effect of such asymmetric Pt_1O_4 coordination on low-temperature CO oxidation was
20 evaluated under an O_2 -rich condition. As shown in Figure 2a, $\text{Pt}_1/\text{CeO}_2_{\text{AT}}$ was inactive
21 below ~ 200 °C and showed better activity than bare CeO_2 only at temperatures above ~ 240
22 °C, which is similar to previous reports.^[3c, 7] In contrast, $\text{Pt}_1/\text{CeO}_2_{\text{TS}}$ showed a significantly
23 enhanced low-temperature activity, evidenced by a significantly lower T_{50} (temperature
24 required for 50 % conversion of CO) of ~ 150 °C compared to ~ 287 °C for $\text{Pt}_1/\text{CeO}_2_{\text{AT}}$
25 (Table S4). It also showed good cycling stability as no deactivation in low-temperature CO

1 oxidation was observed after repeated light-off measurements (Figure 2a). Although the
 2 reductive treatment on Pt₁/CeO₂_AT can enhance the low-temperature performance (i.e.,
 3 decreased T_{10} , T_{50} , and T_{90} in Figure 2b, right) by forming Pt NPs,^[7] the so-called activated
 4 catalyst is susceptible to drastic activity loss (nearly back to the original T_{10} , T_{50} , and T_{90} in
 5 Figure 2b, right) once being oxidized at temperatures > 400 °C.^[2d] This is consistent with
 6 previous experimental observations by Gänzler et al. that redispersion of metallic Pt NPs (< 2
 7 nm) on CeO₂ readily occurred at 400 °C in an oxidizing atmosphere.^[8d] In contrast, very
 8 minor increases in T_{10} , T_{50} , and T_{90} (2-10 °C) were observed for the Pt₁/CeO₂_TS catalyst,
 9 even after being oxidized at 500 °C (Figure 2b, left).



10
 11
 12 **Figure 2.** (a) CO light-off curves collected over as-synthesized Pt₁/CeO₂_AT, Pt₁/CeO₂_TS,
 13 and bare CeO₂ calcined at 800 °C in air. Reaction conditions: 1 % CO, 10 % O₂, with N₂
 14 balance, GHSV of 200 L/g-h. (b) The T_{10} , T_{50} , and T_{90} temperatures (temperatures required
 15 for 10 %, 50 %, and 90 % CO conversions) of Pt₁/CeO₂ catalysts in the as-synthesized state
 16 and after reductive (at 275 °C in 5 % CO for 30 min) and oxidative (at 500 °C in 10 % O₂ for

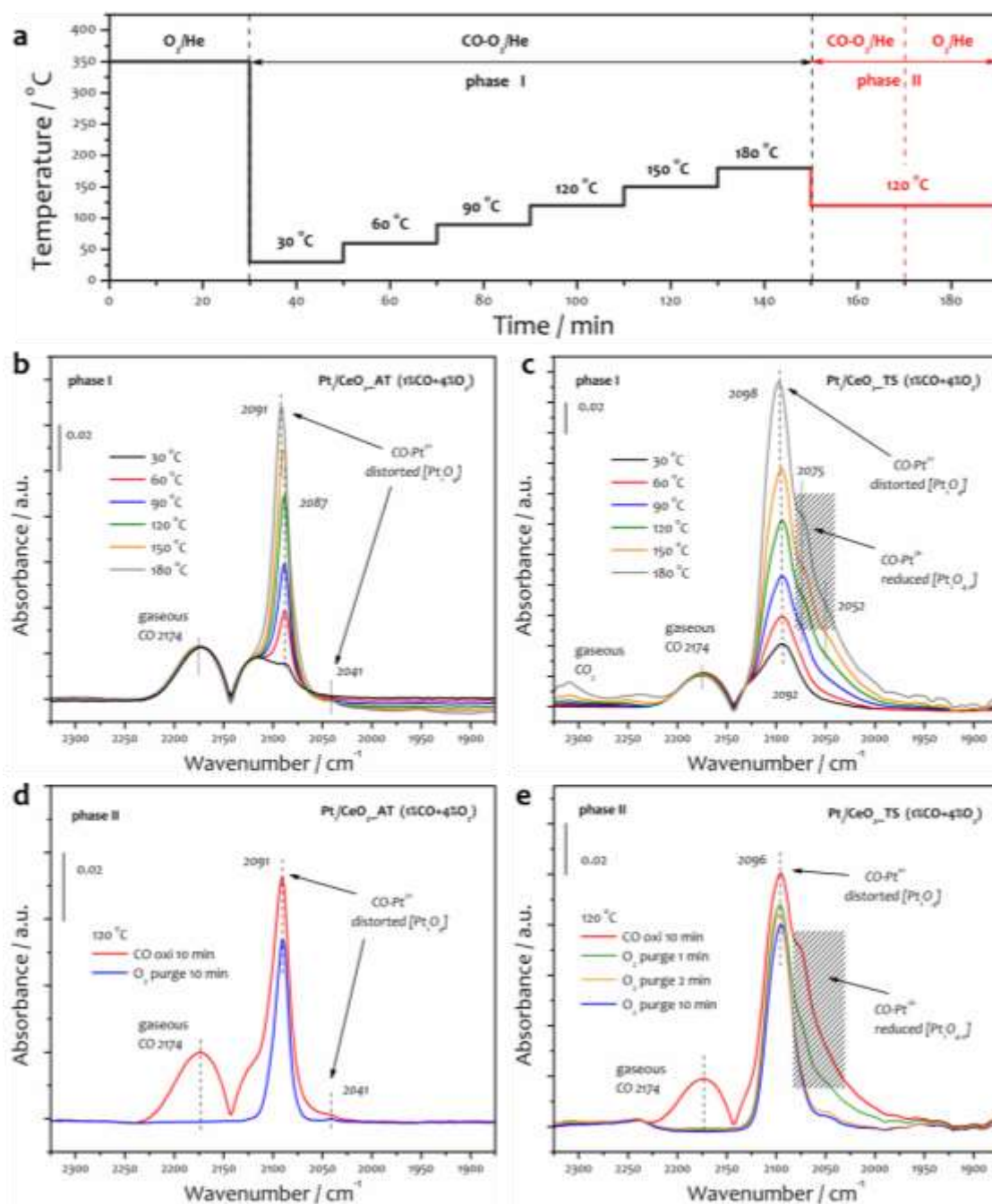
1 2 h) treatments. The dispersion status as well as the local coordinations of Pt atoms at
2 corresponding stages are also illustrated.

3
4 These results clearly confirmed that enhanced low-temperature activity as well as high
5 thermal stability can be achieved in the single-atom Pt₁/CeO₂_TS catalyst. Careful STEM
6 investigations have excluded the morphological effect of the ceria support (Figures 1b-1c, S3-
7 S4) from high-temperature facet reconstruction,^[15] which could influence the Pt-CeO₂
8 interaction as well as O₂ activation during CO oxidation.^[16] Such an enhanced low-
9 temperature CO oxidation activity cannot be solely explained by the higher surface area of
10 Pt₁/CeO₂_TS, which is only ~ 1.5 times that of Pt₁/CeO₂_AT (Table S1). Catalyst reducibility
11 does not appear to induce such a difference, since temperature-programmed reduction in CO
12 indicated that the surface lattice oxygen (O_l) in both catalysts can be readily removed at < 90
13 °C (Figure S7), and in fact, Pt₁/CeO₂_AT even showed a more pronounced low-temperature
14 reducibility possibly due to a stronger Pt-CeO₂ interaction.^[7] Influence of Ce³⁺/V_O (oxygen
15 vacancy) that could be introduced by TS treatment in an inert atmosphere was also excluded
16 by surface sensitive XPS. As-synthesized Pt₁/CeO₂ (AT and TS) catalysts showed similar
17 contents of defect-related O species (7-10 %) and Ce³⁺ ions (16-19 %) on the surface (Figures
18 S5b and S5c).^[7, 17]

19 Kinetic studies were also performed to further understand the effect of the asymmetric
20 coordination environment of Pt²⁺ caused by TS synthesis. Although two Pt₁/CeO₂ catalysts
21 showed similar apparent activation energies (E_a) of 60-70 kJ/mol (Figure S8), they exhibited
22 distinct reaction orders for the reactants (Figure S9). Pt₁/CeO₂_AT showed the order of 0.76
23 for CO and ~ 0 for O₂, while Pt₁/CeO₂_TS showed the order of ~ 0 for both CO and O₂. A
24 similar E_a might suggest a similar mechanism for the two catalysts, while different reaction
25 orders for CO clearly indicate that the kinetic relevance of CO adsorption/activation has been
26 largely weakened for Pt₁/CeO₂_TS. Therefore, it can be reasonably inferred that compared to
27 the over-stabilized Pt²⁺ on CeO₂ via AT, the asymmetric Pt₁O₄ coordination induced by TS

1 renders much enhanced CO activation, and thereby accelerated low-temperature CO oxidation
2 (Figure 2a).

3 Diffuse reflectance infrared Fourier transform spectroscopy (DRIFTS) using CO as a probe
4 molecule is powerful for probing the nature of supported PGM species, as well as the site
5 evolution under reaction conditions.^[1a, 9, 10c, 10e, 10f, 12, 18] Herein, after 350 °C pretreatment in
6 10 % O₂, in situ DRIFTS was performed at different temperatures and conditions over the two
7 Pt₁/CeO₂ catalysts, which can be divided into two consecutive stages (Figure 3a). The phase-I
8 showed CO oxidation in a temperature-programmed manner. In Figure 3b, at 30 °C,
9 Pt₁/CeO₂_AT shows a very weak peak around 2087 cm⁻¹, which has been widely ascribed to
10 CO linearly adsorbed on isolated Pt²⁺ cations.^[1a, 7, 19] Here we tentatively assign this 2087 cm⁻¹
11 peak to CO on isolated Pt²⁺ in a distorted Pt₁O₄ configuration, since both computational and
12 surface science studies have suggested that perfect square-planar Pt₁O₄ hardly chemisorbs CO
13 even at -150 °C.^[3b, 6, 20] The low intensity of the 2087 cm⁻¹ peak indicates that Pt²⁺ in
14 Pt₁/CeO₂_AT presents a near-perfect square-planar Pt₁O₄ coordination environment, which is
15 consistent with our EXAFS analysis (Figure 1e and Table 1) as well as the pulsed CO
16 chemisorption result showing a weak CO uptake (2.6 % of the amount of loaded Pt atoms) at
17 30 °C (Figure S10). Notably, the intensity of this CO-Pt²⁺ peak at ~ 2090 cm⁻¹ increases as the
18 temperature increases up to 180 °C (Figure 3b), suggesting a more pronounced distortion of
19 the Pt₁O₄ configuration (an increased coordination asymmetry) under CO oxidation at
20 elevated temperatures, which can also be traced by the slight peak shift to higher
21 wavenumbers. Very recently, slight distortion and displacement of Pt²⁺ upon CO
22 chemisorption was also suggested by Maurer et al. based on combined UHV-FTIRS and
23 DRIFTS studies over a steam-treated Pt₁/CeO₂ catalyst.^[3e] More intense perturbations of the
24 local structure by CO has been observed for supported Pd in the forms of both single atoms
25 and NPs.^[10e, 21]



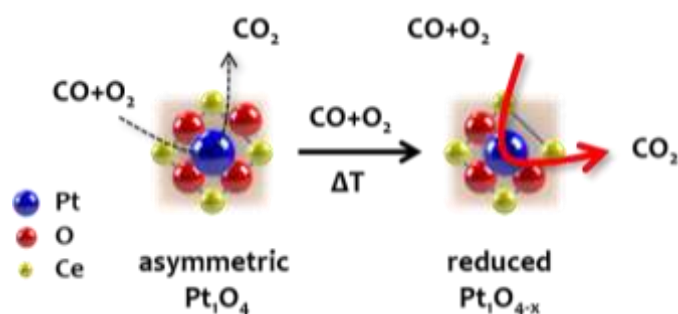
1
2
3 **Figure 3.** (a) In situ diffuse reflectance infrared Fourier transform spectroscopy (DRIFTS)
4 measurements over Pt₁/CeO₂_AT and Pt₁/CeO₂_TS catalysts under CO oxidation (1 % CO,
5 4 % O₂, He balance, 60 ml/min) and oxidizing (4 % O₂, He balance, 60 ml/min) conditions.
6 Ramping rate: 20 °C/min. DRIFTS spectra recorded at different temperatures (30-180 °C)
7 under CO oxidation in phase-I over Pt₁/CeO₂_AT (b) and Pt₁/CeO₂_TS (c) catalysts. DRIFTS
8 recorded at 120 °C in phase-II over Pt₁/CeO₂_AT (d) and Pt₁/CeO₂_TS (e) catalysts under CO
9 oxidation followed by purging in O₂/He.

10
11 In contrast, Pt₁/CeO₂_TS shows one symmetric while more intense CO-Pt²⁺ IR peak at a
12 slightly higher wavenumber of 2092 cm⁻¹ when flowing CO and O₂ at 30 °C (Figure 3c). This
13 also confirms the generation of isolated Pt²⁺ with an asymmetric Pt₁O₄ geometry by the TS

1 synthesis, in accordance with the increased CO uptake (29 % of loaded Pt atoms) at 30 °C
2 compared to that (2.6 % of loaded Pt) for Pt₁/CeO₂_AT (Figure S10). The slightly different
3 peak positions (2092 vs. 2087 cm⁻¹) in the two catalysts also indicate different local
4 environments (e.g., location, coordination) of isolated Pt²⁺ that lead to different Pt-CeO₂/CO-
5 Pt²⁺ interactions in the two catalysts. The broader peak in Pt₁/CeO₂_TS also suggests a wider
6 distribution of local environments of Pt²⁺, as expected for TS synthesis which involves the
7 intense surface reconstruction of CeO₂ and limits the vapor-phase transport of PtO₂ to the
8 most thermodynamically stable sites on CeO₂ surface (Figure 1a). The enhanced CO-Pt²⁺
9 peak intensity with slight peak blueshift was also observed at elevated temperatures over
10 Pt₁/CeO₂_TS (Figure 3c). Interestingly, distinct from Pt₁/CeO₂_AT, Pt₁/CeO₂_TS shows two
11 additional shoulder-like features around 2075 and 2052 cm⁻¹ at temperatures ≥ 90 °C (Figure
12 3c). The two evolved species are not associated with either metallic Pt⁰ clusters/NPs, which
13 should show lower-wavenumber features (< 2000 cm⁻¹) on extended Pt surfaces (Figure S11),
14 or oxidized PtO_x clusters, which would show a higher-wavenumber feature (> 2100 cm⁻¹).^{[4a,}
15 ^{8b, 12]} Here, they are indexed as atop CO on the partially reduced Pt₁^{δ+} atoms with Pt₁O_{4-x} local
16 coordinations.^[10c] Recently, Wang et al., based on combined DFT calculations and *ab initio*
17 atomistic thermodynamics modeling, demonstrated that mono-dispersed Pt⁰ are
18 thermodynamically unstable compared to bulk Pt⁰, also supporting our assignment of these
19 shoulder features to partially reduced Pt₁^{δ+} species.^[22]

20 To evaluate the reactivities of different Pt₁ species, after CO oxidation up to 180 °C in
21 phase-I, the catalysts were cooled down to 120 °C in the same CO + O₂ atmosphere followed
22 by purging in O₂/He (phase-II of Figure 3a). As expected for Pt₁/CeO₂_AT, the CO-Pt²⁺
23 (2091 cm⁻¹) peak decreased very slightly after CO was discontinued (Figure 3d), consistent
24 with the lack of low-temperature activity below 200 °C (Figure 2a). This is also consistent
25 with the CO-DRIFTS results in previous reports.^[3c, 7, 19] Identical experiments were also

1 conducted on Pt₁/CeO₂_TS (Figure 3e). Notably, in contrast to CO on isolated Pt²⁺ (2096 cm⁻¹)
 2 ¹) that was only slightly removed by O₂ purging for 10 min, CO on the partially reduced Pt₁^{δ+}
 3 species (i.e., 2075 and 2052 cm⁻¹ shoulder) got rapidly removed within 2 min (Figure 3e).
 4 Given that the light-off curve of CO oxidation over Pt₁/CeO₂_TS shows an onset at ~ 70 °C
 5 (Figure 2a), the excellent low-temperature activity is attributed to the reaction-induced Pt₁^{δ+}
 6 species in the reduced Pt₁O_{4-x} coordination. Careful AC-STEM investigations of the
 7 Pt₁/CeO₂_TS catalyst after the phase-I CO-DRIFTS experiments (Figure 3a) excluded the
 8 presence of Pt clusters/NPs (Figure S12), indicating that the shoulder IR features (2075 and
 9 2052 cm⁻¹) should not be associated with Pt clusters/NPs transformed from isolated Pt²⁺. This
 10 was further confirmed by additional CO-DRIFTS measurements that the shoulder species can
 11 be eliminated by treatment in O₂/He at 250 °C, which cannot redisperse the reduction-induced
 12 metallic Pt clusters/NPs (requiring oxidizing treatment > 400 °C) (Figure S13).^[8d]
 13 Synchrotron-based EXAFS analysis also confirmed the absence of Pt-Pt bonding, i.e.,
 14 formation of Pt/PtO_x clusters/NPs, in the spent Pt₁/CeO₂_TS catalyst after IR measurements
 15 (Figure S14). XPS of the same spent Pt₁/CeO₂_TS catalyst after IR measurement also
 16 excluded the evolution of metallic Pt⁰ species after CO oxidation (Figure S15a). The partially
 17 reduced Pt states may not be able to be tracked by ex-situ XPS given that CO on the evolved
 18 Pt₁O_{4-x} species can be readily replaced by gaseous O₂. However, an increased amount of
 19 defect-related O species (15.7 %) was present on the surface of the spent Pt₁/CeO₂_TS (Figure
 20 S15b), suggesting that Pt₁O₄ was partially reduced during CO oxidation.



1 **Figure 4.** Schematic of the proposed dynamic evolution of the local environments of isolated
2 Pt^{2+} in Pt_1/CeO_2 _TS from an asymmetric (distorted) Pt_1O_4 to the partially reduced $\text{Pt}_1\text{O}_{4-x}$ for
3 greatly enhanced low-temperature CO oxidation.

4
5 The DRIFTS results (Figure 3e) indicate that the reaction-induced $\text{Pt}_1^{\delta+}$ species in
6 Pt_1/CeO_2 _TS are much more reactive than as-synthesized Pt^{2+} in Pt_1/CeO_2 _AT during low-
7 temperature CO oxidation (Figure 3d), which also agree with the distinct reaction orders with
8 respect to CO for Pt_1/CeO_2 _TS (0.76) and Pt_1/CeO_2 _AT (~ 0) (Figure S9). Here, both
9 Pt_1/CeO_2 _AT and Pt_1/CeO_2 _TS showed an increasingly pronounced Pt_1O_4 distortion during
10 CO oxidation at elevated temperatures (Figures 3b and 3c), except that the reduced $\text{Pt}_1^{\delta+}$ was
11 only formed over Pt_1/CeO_2 _TS. The formation of the partially reduced $\text{Pt}_1^{\delta+}$ species induced
12 by the reaction is therefore ascribed to the tailored local environments (e.g., location,
13 coordination) of Pt^{2+} single atoms produced by TS, as evidenced by the decreased Pt_1O_4
14 coordination symmetry (Figure 1d and Table 1) as well as the different vibrational frequency
15 of CO- Pt^{2+} compared to those produced by AT (Figures 3b and 3c).

16 Based on above discussion, the dynamic behavior of isolated Pt^{2+} in Pt_1/CeO_2 _TS during
17 CO oxidation is depicted (Figure 4), which we postulate is a result of an asymmetric Pt_1O_4
18 coordination produced by TS in contrast to a highly symmetric square-planar Pt_1O_4
19 coordination by AT rendering over-stabilized Pt^{2+} single atoms. During CO oxidation, Pt^{2+} in
20 Pt_1/CeO_2 _TS dynamically adopts a partially reduced $\text{Pt}_1\text{O}_{4-x}$ coordination. Due to the reduced
21 electronic states, the evolved $\text{Pt}_1^{\delta+}$ species greatly promote CO oxidation at low temperatures,
22 showing an exceptional activity comparable to that of clusters/NPs-containing Pt/CeO₂
23 catalysts (Figure S16).^[3g, 23] More importantly, while metallic Pt undergoes
24 oxidation/dispersion leading to a drastic activity loss once being oxidized at 500 °C,
25 Pt_1/CeO_2 _TS retains its reactivity (Figure 2b). The dynamically interconnected charge states
26 of isolated Pt on CeO₂ (100) surface which is phonon-assisted as identified by combined DFT
27 and first-principles molecular dynamics studies helps explain our experimental findings.^[3h]

1 These results here demonstrate that the thermally stable Pt₁/CeO₂ catalyst directly synthesized
2 by a thermal-shock method is low-temperature active for CO oxidation due to the tailored
3 local environments of isolated Pt²⁺ that is different from that achieved by atom trapping which
4 tends to place Pt in sites that are stable but unreactive.

5 **3. Conclusion**

6 In summary, atomically dispersed Pt on CeO₂ with tailored local coordination structures
7 and electronic states were generated via two different high-temperature synthesis approaches,
8 namely atom-trapping (AT) and thermal-shock (TS) synthesis. Complementary STEM, XAS,
9 *in situ* DRIFTS, and CO chemisorption studies confirmed that in contrast to AT synthesis that
10 resulted in over-stabilized Pt²⁺ single atoms on CeO₂ with a near-perfect square-planar Pt₁O₄
11 coordination with a high geometric symmetry, TS synthesis in an inert atmosphere stabilized
12 isolated Pt²⁺ in an asymmetric Pt₁O₄ configuration by inducing intense surface reconstruction
13 of CeO₂ meanwhile limiting the vapor-phase transport of PtO₂. Benefiting from such an
14 asymmetric coordination, active Pt₁^{δ+} species in partially reduced Pt₁O_{4-x} coordination were
15 formed during CO oxidation, leading to the greatly enhanced low-temperature activity
16 evidenced by a decrease of T₅₀ by ~ 140 °C at a high space velocity of 200 L/g-h. The
17 findings here show that there is room to engineer the active sites in Pt/CeO₂ catalysts via
18 novel synthesis methods. Comparing the behavior of Pt single atoms in different local
19 environment helps provide insights into the structure-function relationship of SACs revealing
20 dynamic site evolution as well as site-dependent reactivity that is coordination sensitive.

21 **Supporting Information**

22 Supporting Information is available from the Wiley Online Library or from the author.
23

24 **Acknowledgements**

25 This work was supported by U.S. Department of Energy (DOE), Office of Basic Energy
26 Sciences (SC), Division of Chemical Sciences (grant DE-FG02-05ER15712). K.K. and C.E.G
27 would like to acknowledge additional support from U.S. DOE, Energy Efficiency and
28 Renewable Energy, Vehicle Technology Office for part of the IR experiments. Use of the

1 Advanced Photon Source is supported by the U.S. Department of Energy, Office of Science,
2 Office of Basic Energy Sciences, under Contract No. DE-AC02-06CH11357, and the
3 Canadian Light Source and its funding partners. Use of the Stanford Synchrotron Radiation
4 Lightsource, SLAC National Accelerator Laboratory, is supported by the U.S. Department of
5 Energy, Office of Science, Office of Basic Energy Sciences under Contract No. DE-AC02-
6 76SF00515. G. W. would like to acknowledge additional support from U.S. DOE, Energy
7 Efficiency and Renewable Energy, Vehicle Technology Office. XPS measurements were
8 performed using EMSL (grid.436923.9), a DOE Office of Science User Facility sponsored by
9 the Office of Biological and Environmental Research. We acknowledge Dr. Fengyuan Shi at
10 UIC for performing STEM imaging. This work made use of instruments in the Electron
11 Microscopy Core of UIC's Research Resources Center. We also would like to thank Dr. Jiyun
12 Hong for preparing the sample for XAS of the spent Pt₁/CeO₂_TS catalyst at SSRL.

13
14 Received: ((will be filled in by the editorial staff))

15 Revised: ((will be filled in by the editorial staff))

16 Published online: ((will be filled in by the editorial staff))

17
18 References

- 19 [1] a J. Jones, H. Xiong, A. T. DeLaRiva, E. J. Peterson, H. Pham, S. R. Challa, G. Qi, S.
20 Oh, M. H. Wiebenga, X. I. P. Hernández, *Science* **2016**, *353*, 150-154; b B. Qiao, A.
21 Wang, X. Yang, L. F. Allard, Z. Jiang, Y. Cui, J. Liu, J. Li, T. Zhang, *Nat. Chem.*
22 **2011**, *3*, 634-641; c J. Shan, M. Li, L. F. Allard, S. Lee, M. Flytzani-Stephanopoulos,
23 *Nature* **2017**, *551*, 605-608; d L. Cao, W. Liu, Q. Luo, R. Yin, B. Wang, J.
24 Weissenrieder, M. Soldemo, H. Yan, Y. Lin, Z. Sun, C. Ma, W. Zhang, S. Chen, H.
25 Wang, Q. Guan, T. Yao, S. Wei, J. Yang, J. Lu, *Nature* **2019**, *565*, 631-635; e B.-H.
26 Lee, S. Park, M. Kim, A. K. Sinha, S. C. Lee, E. Jung, W. J. Chang, K.-S. Lee, J. H.
27 Kim, S.-P. Cho, *Nat. Mater.* **2019**, *18*, 620-626; f C. Zhu, S. Fu, Q. Shi, D. Du, Y. Lin,
28 *Angew. Chem. Int. Ed.* **2017**, *56*, 13944-13960.
- 29 [2] a M. Cargnello, V. V. Doan-Nguyen, T. R. Gordon, R. E. Diaz, E. A. Stach, R. J.
30 Gorte, P. Fornasiero, C. B. Murray, *Science* **2013**, *341*, 771-773; b C. K. Lambert,
31 *Nat. Catal.* **2019**, *2*, 554-557; c A. Beniya, S. Higashi, *Nat. Catal.* **2019**, *2*, 590-602; d
32 A. K. Datye, M. Votsmeier, *Nat. Mater.* **2020**, 1-11.
- 33 [3] a D. Kunwar, S. Zhou, A. De La Riva, E. Peterson, H. Xiong, X. I. Pereira Hernandez,
34 S. C. Purdy, R. ter Veen, H. H. Brongersma, J. T. Miller, H. Hashiguchi, L. Kovarik,
35 S. Lin, H. Guo, Y. Wang, A. Datye, *ACS Catal.* **2019**, *9*, 3978-3990; b F. Dvořák, M.
36 F. Camellone, A. Tovt, N.-D. Tran, F. R. Negreiros, M. Vorokhta, T. Skála, I.
37 Matolínová, J. Mysliveček, V. Matolín, *Nat. Commun.* **2016**, *7*, 10801; c L. Nie, D.
38 Mei, H. Xiong, B. Peng, Z. Ren, X. I. P. Hernandez, A. DeLaRiva, M. Wang, M. H.
39 Engelhard, L. Kovarik, *Science* **2017**, *358*, 1419-1423; d G. Ferré, M. Aouine, F.
40 Bosselet, L. Burel, F. J. Cadete Santos Aires, C. Geantet, S. Ntais, F. Maurer, M.
41 Casapu, J. D. Grunwaldt, T. Epicier, S. Loricant, P. Vernoux, *Catal. Sci. Technol.*
42 **2020**, *10*, 3904-3917; e F. Maurer, J. Jelic, J. Wang, A. Gänzler, P. Dolcet, C. Wöll, Y.
43 Wang, F. Studt, M. Casapu, J.-D. Grunwaldt, *Nat. Catal.* **2020**, *3*, 824-833; f A. J.
44 Therrien, A. J. Hensley, M. D. Marcinkowski, R. Zhang, F. R. Lucci, B. Coughlin, A.
45 C. Schilling, J.-S. McEwen, E. C. H. Sykes, *Nat. Catal.* **2018**, *1*, 192-198; g J.
46 Resasco, L. DeRita, S. Dai, J. P. Chada, M. Xu, X. Yan, J. Finzel, S. Hanukovich, A.
47 S. Hoffman, G. W. Graham, S. R. Bare, X. Pan, P. Christopher, *J. Am. Chem. Soc.*
48 **2019**, *142*, 169-184; h N. Daelman, M. Capdevila-Cortada, N. López, *Nat. Mater.*
49 **2019**, *18*, 1215-1221.

- 1 [4] a P. Xie, T. Pu, A. Nie, S. Hwang, S. C. Purdy, W. Yu, D. Su, J. T. Miller, C. Wang,
2 *ACS Catal.* **2018**, *8*, 4044-4048; b R. Lang, W. Xi, J.-C. Liu, Y.-T. Cui, T. Li, A. F.
3 Lee, F. Chen, Y. Chen, L. Li, L. Li, J. Lin, S. Miao, X. Liu, A.-Q. Wang, X. Wang, J.
4 Luo, B. Qiao, J. Li, T. Zhang, *Nat. Commun.* **2019**, *10*, 234; c D. Yan, J. Chen, H.-P.
5 Jia, *Angew. Chem. Int. Ed.* **2020**, *59*, 13562–13567.
- 6 [5] a H. A. Aleksandrov, K. M. Neyman, G. N. Vayssilov, *Phys. Chem. Chem. Phys.*
7 **2015**, *17*, 14551-14560; b Y. Lykhach, A. Figueroba, M. F. Camellone, A. Neitzel, T.
8 Skála, F. R. Negreiros, M. Vorokhta, N. Tsud, K. C. Prince, S. Fabris, K. M. Neyman,
9 V. Matolín, J. Libuda, *Phys. Chem. Chem. Phys.* **2016**, *18*, 7672-7679.
- 10 [6] a A. Bruix, Y. Lykhach, I. Matolínová, A. Neitzel, T. Skála, N. Tsud, M. Vorokhta, V.
11 Stetsovych, K. Ševčíková, J. Mysliveček, *Angew. Chem. Int. Ed.* **2014**, *53*, 10525-
12 10530; b A. Neitzel, Y. Lykhach, T. Skála, N. Tsud, M. Vorokhta, D. Mazur, K. C.
13 Prince, V. Matolín, J. Libuda, *Phys. Chem. Chem. Phys.* **2014**, *16*, 24747-24754; c Y.
14 Tang, Y.-G. Wang, J. Li, *J. Phys. Chem. C* **2017**, *121*, 11281-11289.
- 15 [7] X. I. Pereira-Hernández, A. DeLaRiva, V. Muravev, D. Kunwar, H. Xiong, B.
16 Sudduth, M. Engelhard, L. Kovarik, E. J. Hensen, Y. Wang, *Nat. Commun.* **2019**, *10*,
17 1358.
- 18 [8] a X. Liu, S. Jia, M. Yang, Y. Tang, Y. Wen, S. Chu, J. Wang, B. Shan, R. Chen, *Nat.*
19 *Commun.* **2020**, *11*, 4240; b H. Wang, J.-X. Liu, L. F. Allard, S. Lee, J. Liu, H. Li, J.
20 Wang, J. Wang, S. H. Oh, W. Li, *Nat. Commun.* **2019**, *10*, 1-12; c Y. Lu, C.
21 Thompson, D. Kunwar, A. Datye, A. M. Karim, *ChemCatChem* **2020**, *12*, 1726-1733;
22 d A. M. Gänzler, M. Casapu, P. Vernoux, S. Lorient, F. J. Cadete Santos Aires, T.
23 Epicier, B. Betz, R. Hoyer, J. D. Grunwaldt, *Angew. Chem. Int. Ed.* **2017**, *56*, 13078-
24 13082.
- 25 [9] a L. DeRita, S. Dai, K. Lopez-Zepeda, N. Pham, G. W. Graham, X. Pan, P.
26 Christopher, *J. Am. Chem. Soc.* **2017**, *139*, 14150-14165; b H. V. Thang, G.
27 Pacchioni, L. DeRita, P. Christopher, *J. Catal.* **2018**, *367*, 104-114.
- 28 [10] a M. J. Kale, P. Christopher, *ACS Catal.* **2016**, *6*, 5599-5609; b K. Alexopoulos, Y.
29 Wang, D. G. Vlachos, *ACS Catal.* **2019**, *9*, 5002-5010; c L. DeRita, J. Resasco, S. Dai,
30 A. Boubnov, H. V. Thang, A. S. Hoffman, I. Ro, G. W. Graham, S. R. Bare, G.
31 Pacchioni, *Nat. Mater.* **2019**, *18*, 746-751; d Y. Tang, C. Asokan, M. Xu, G. W.
32 Graham, X. Pan, P. Christopher, J. Li, P. Sautet, *Nat. Commun.* **2019**, *10*, 1-10; e D.
33 Jiang, G. Wan, C. E. Garcia Vargas, L. Li, X. I. Pereira Hernandez, C. Wang, Y.
34 Wang, *ACS Catal.* **2020**, *10*, 11356-11364; f T. Avanesian, S. Dai, M. J. Kale, G. W.
35 Graham, X. Pan, P. Christopher, *J. Am. Chem. Soc.* **2017**, *139*, 4551-4558; g L. Liu,
36 D. M. Meira, R. Arenal, P. Concepcion, A. V. Puga, A. Corma, *ACS Catal.* **2019**, *9*,
37 10626-10639.
- 38 [11] a Y. Yao, Z. Huang, P. Xie, S. D. Lacey, R. J. Jacob, H. Xie, F. Chen, A. Nie, T. Pu,
39 M. Rehwoldt, D. Yu, M. R. Zachariah, C. Wang, R. Shahbazian-Yassar, J. Li, L. Hu,
40 *Science* **2018**, *359*, 1489-1494; b Y. Yao, Z. Huang, P. Xie, L. Wu, L. Ma, T. Li, Z.
41 Pang, M. Jiao, Z. Liang, J. Gao, Y. He, D. J. Kline, M. R. Zachariah, C. Wang, J. Lu,
42 T. Wu, T. Li, C. Wang, R. Shahbazian-Yassar, L. Hu, *Nature Nanotechnol.* **2019**, *14*,
43 851-857; c Y. Yao, Z. Huang, T. Li, H. Wang, Y. Liu, H. S. Stein, Y. Mao, J. Gao, M.
44 Jiao, Q. Dong, J. Dai, P. Xie, H. Xie, S. D. Lacey, I. Takeuchi, J. M. Gregoire, R.
45 Jiang, C. Wang, A. D. Taylor, R. Shahbazian-Yassar, L. Hu, *Proc. Natl. Acad. Sci.*
46 **2020**, *117*, 6316-6322.
- 47 [12] M. Kottwitz, Y. Li, R. M. Palomino, Z. Liu, G. Wang, Q. Wu, J. Huang, J.
48 Timoshenko, S. D. Senanayake, M. Balasubramanian, D. Lu, R. G. Nuzzo, A. I.
49 Frenkel, *ACS Catal.* **2019**, *9*, 8738-8748.
- 50 [13] A. Ankudinov, J. Rehr, J. Low, S. Bare, *Top. Catal.* **2002**, *18*, 3-7.
- 51 [14] A. Ankudinov, J. Rehr, J. J. Low, S. R. Bare, *J. Chem. Phys.* **2002**, *116*, 1911-1919.

- 1 [15] a C. Yang, X. Yu, S. Heißler, A. Nefedov, S. Colussi, J. Llorca, A. Trovarelli, Y.
2 Wang, C. Wöll, *Angew. Chem. Int. Ed.* **2017**, *56*, 375-379; b C. Yang, M. Capdevila-
3 Cortada, C. Dong, Y. Zhou, J. Wang, X. Yu, A. Nefedov, S. Heißler, N. López, W.
4 Shen, C. Wöll, Y. Wang, *J. Phys. Chem. Lett.* **2020**, *11*, 7925-7931.
- 5 [16] a C. Yang, X. Yu, S. Heissler, P. G. Weidler, A. Nefedov, Y. Wang, C. Woell, T.
6 Kropp, J. Paier, J. Sauer, *Angew. Chem. Int. Ed.* **2017**, *56*, 16399-16404; b D. Jiang,
7 W. Wang, L. Zhang, Y. Zheng, Z. Wang, *ACS Catal.* **2015**, 4851-4858; c F. Polo-
8 Garzon, Z. Bao, X. Zhang, W. Huang, Z. Wu, *ACS Catal.* **2019**, *9*, 5692-5707; d G.
9 Spezzati, A. Benavidez, A. T. DeLaRiva, Y. Su, J. P. Hofmann, S. Asahina, E. J.
10 Olivier, J. H. Neethling, J. T. Miller, A. K. Datye, E. J. M. Hensen, *Appl. Catal. B:*
11 *Environ.* **2018**, *243*, 36-46.
- 12 [17] a D. Jiang, W. Wang, L. Zhang, R. Qiu, S. Sun, Y. Zheng, *Appl. Catal. B: Environ.*
13 **2015**, *165*, 399-407; b D. Jiang, W. Wang, Y. Zheng, L. Zhang, *Appl. Catal. B:*
14 *Environ.* **2016**, *191*, 86-93; c D. Jiang, W. Wang, E. Gao, S. Sun, L. Zhang, *Chem.*
15 *Commun.* **2014**, *50*, 2005-2007.
- 16 [18] a D. Daniel, *J. Phys. Chem.* **1988**, *92*, 3891-3899; b J. Ke, W. Zhu, Y. Jiang, R. Si, Y.-
17 J. Wang, S.-C. Li, C. Jin, H. Liu, W.-G. Song, C.-H. Yan, *ACS Catal.* **2015**, *5*, 5164-
18 5173; c C. Lentz, S. P. Jand, J. Melke, C. Roth, P. Kaghazchi, *J. Mol. Catal. A Chem.*
19 **2017**, *426*, 1-9; d Y. Lykhach, A. Bruix, S. Fabris, V. Potin, I. Matolínová, V.
20 Matolín, J. Libuda, K. M. Neyman, *Catal. Sci. Technol.* **2017**, *7*, 4315-4345.
- 21 [19] K. Ding, A. Gulec, A. M. Johnson, N. M. Schweitzer, G. D. Stucky, L. D. Marks, P.
22 C. Stair, *Science* **2015**, *350*, 189-192.
- 23 [20] H. A. Aleksandrov, K. M. Neyman, K. I. Hadjiivanov, G. N. Vayssilov, *Phys. Chem.*
24 *Chem. Phys.* **2016**, *18*, 22108-22121.
- 25 [21] M. A. Newton, C. Belder-Coldeira, A. Martínez-Arias, M. Fernández-García, *Nat.*
26 *Mater.* **2007**, *6*, 528-532.
- 27 [22] X. Wang, J. A. van Bokhoven, D. Palagin, *Phys. Chem. Chem. Phys.* **2020**, *22*, 28-38.
- 28 [23] K. An, S. Alayoglu, N. Musselwhite, S. Plamthottam, G. Melaet, A. E. Lindeman, G.
29 A. Somorjai, *J. Am. Chem. Soc.* **2013**, *135*, 16689-16696.
- 30

31

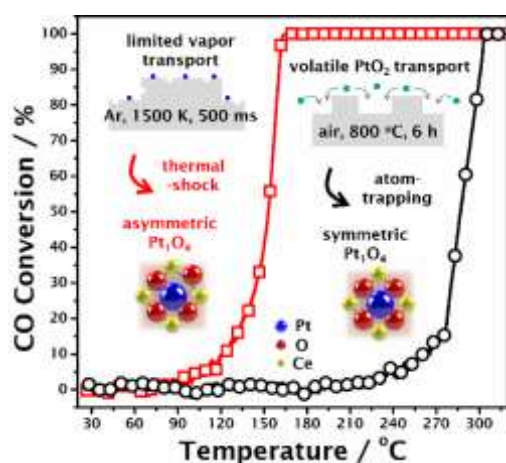
32

33

1 Highly active and robust single-atom Pt₁/CeO₂ catalyst for CO oxidation is developed by
2 tailoring the local environment of isolated Pt²⁺ via thermal-shock synthesis. Ultrafast
3 shockwaves in an inert atmosphere generate Pt single atoms in an asymmetric Pt₁O₄
4 configuration, resulting in greatly enhanced low-temperature activity that is retained under
5 oxidizing conditions.

6
7
8 *Dong Jiang,¹ Yonggang Yao,² Tangyuan Li,² Gang Wan,³ Xavier Isidro Pereira-Hernández,¹*
9 *Yubing Lu,⁴ Jinshu Tian,⁴ Konstantin Khivantsev,⁴ Mark H. Engelhard,⁴ Chengjun Sun,⁵*
10 *Carlos E. García-Vargas,¹ Adam S. Hoffman,³ Simon R. Bare,³ Abhaya K. Datye,^{6*} Liangbing*
11 *Hu,^{2*} and Yong Wang^{1,4*}*

14 Tailoring the Local Environment of Platinum in Single-Atom Pt₁/CeO₂ Catalysts for 15 Robust Low-Temperature CO Oxidation



18
19